Adhesion Control for Micro- and Nanomanipulation

Jérôme Dejeu,[†,*] Mikhael Bechelany,[‡,§] Patrick Rougeot,[†] Laëtitia Philippe,[§] and Michaël Gauthier[†,*]

[†]FEMTO-ST Institute, AS2M Department, UMR CNRS 6174-UFC/ENSMM/UTBM, 24 rue Alain Savary, 25000 Besançon, France, [‡]Institut Européen des Membranes de Montpellier (IEMM, UMR CNRS 5635, ENSCM), Place Eugène Bataillon, 34095 MONTPELLIER Cedex 5, France, and [§]EMPA, Materials Science & Technology, Laboratory for Mechanics of Materials and Nanostructures, Feuerwerkerstrasse 39, CH-3602 Thun, Switzerland

ABSTRACT The adhesion between a micro/nano-object and a microgripper end-effector is an important problem in micromanipulation. Canceling or reducing this force is a great challenge. This force is directly linked to the surface chemical structure of the object and the gripper. We propose to predict this force between a structuring surface and a micro-object with a multisphere van der Waals force model. The surface was structured by polystyrene latex particles (PS particles) with radii from 35 to 2000 nm. The model was compared with experimental pull-off force measurements performed by AFM with different natures of spheres materials glued on the tipless. A wide range of applications, in the field of telecommunications, bioengineering, and more generaly speaking MEMS can be envisaged for these substrates.

KEYWORDS: surface structuring · adhesion force · pull-off force · PS latex particle · micromanipulation · grippers · nanomanipulation

Manufactured products are getting smaller and smaller and are integrating more and more functionalities in small volumes. Several application fields are affected such as bioengineering, telecommunications, or more generally speaking the micro-electromechanical systems (MEMS). The assembly of these microproducts is a great challenge because of the microscopic size of the components.[1] In fact, the major difficulty of micro/nanoassembly comes from the particularity of the micro/nano-objects behavior which depends on surface forces.[2−4] The manipulation of a micro-object requires handling, positioning, and releasing it without disturbances of the surface forces such as electrostatic, van der Waals, or capillary forces.

Current microhandling methods are able to improve micromanipulation but the object behavior is always disturbed by adhesion and thus the repeatability and reliability is still low.[5,6] The required force to separate two surfaces is commonly called the "pull-off" force. The "pull-in" force is the attractive force between two objects when they approach closely. The pull-off force is not well understood and must be studied further to enable the advent of reliable micromanipulation techniques. Current methods to measure micro/nanoforces between surfaces are the surface force apparatus (SFA),[7,8] the atomic force microscope (AFM),[9−11] capacitive force sensors,[12] or nanoindentation testers.[13,14] The modeling of pull-off force is mainly based on the different approaches based on the surface energies on the contact,[15−18] on the integration of the van der Waals forces between objects,[19−22] or on some hybrid approaches between both.[23,24] The adhesion force reduction was already obtained in liquid and dry medium by surface structuring[24−26] or chemical functionalization.[9,27−29] The last technique allows the switch of the force from attractive to repulsive by pH solution modification and improves the micro-object manipulation.[27,30,31] In the case of randomly rough surfaces, the fractal approach is one of the most usual ways to predict wear, adhesion force, or interaction forces.[32−34]

Thanks to the surface structuring, we can reduce the contact area between the gripper and the objects, and in turn this will decrease the contact area and van der Waals forces. Also, we can induce specific properties of the gripper such as using electrically conductive materials to minimize electrostatic force. In practice, the approach for surface structuring can be categorized into two directions: top-down and bottom-up approaches. Top-down approaches encompass template-based techniques[35] and plasma treatment of the surfaces.[36] Bottom-up approaches involve mostly self-assembly and self-organization[37] as for instance chemical deposition,[38] layer-by-layer (LBL) deposition,[39] and colloidal assemblies.[40] There are also methods based on the combination of both bottom-up and top-down approaches, for example, the casting of polymer solution and phase separation,[41] and electrospinning.[42] Among these methods, the application using two-dimensional (2D) colloidal

* Address correspondence to jerome.dejeu@univ-fcomte.fr.

Received for review February 3, 2011 and accepted May 31, 2011.

Published online May 31, 2011
10.1021/nn200658z

crystals, called "natural lithography", which has been suggested by Deckman and Dunsmuir,[43] has attracted attention because it is a relatively easy process in comparison with conventional lithography technique.[43] On the basis of such a process, uniformly sized microstructures and nanostructures could be produced on a substrate using mono- or multilayer colloidal spheres. In recent years, various techniques, based on "nanosphere lithography", have been reported for nano/microfabrication or nano/micropatterning of a wide variety of solid substrates including metals,[44−48] semiconductors,[49,50] and ceramics.[51]

Recently, we reported structuring a surface by nanospheres lithography and measuring the adhesion force. We proposed a multisphere van der Waals force model which may suggest the existence of an optimal value of the sphere radius which minimizes the adhesion. In the case of the 20 μm borosilicate sphere diameter, the pull-off force is reduced to 20 nN by the PS particles layer with a radius of 45 nm.[26] The aim of this paper is to extend this model and to demonstrate the existence of a minimum independent of the diameter and nature of the spheres. First, an improved model compared to our previous paper[26] is going to be proposed and then the parameters of diameter and nature of the spheres are studied. The analysis of the correlation between the experimental measures and the model and a discussion on the application relevance in micromanipulation tasks are performed. The paper is concluded by the surface patterning method and the adhesion measurement methodology.

MODEL DEVELOPMENT

Usually force measurements are conducted between a sphere and a planar substrate where the contact surface is necessary a unique surface. In our case, the substrate is structured with several microspheres and the contact numbers must be studied.

Let us consider the arrangement described in Figure 1 which represents the position of the PS sphere on the substrate (noted S_b). In an application case and also during force measurements the location of the sphere on the probe up the structured surface cannot be controlled precisely. When the probe with a sphere, (noted S_a), is approaching, it touches the nanospheres r_2 (Figure 2) on a noncontrol position. Two extreme cases are considered: (1) The probe r_1 is perfectly aligned with one sphere r_2 (*e.g.*, the sphere $i = 0, j = 0$); it generates only one contact point. This case induces the minimal force between the probe and the nanostructured surface. (2) The probe r_1 is up to the centroid of three adjacent spheres r_2 (*e.g.*, the sphere $i = 0, j = 0$; $i = 0, j = 1$; $i = 1, j = 1$); it generates three contact points which maximize the interaction force between the probe and the nanostructured surface.

The objective of the model is to predict the adhesion force between the nanostructured surface and the

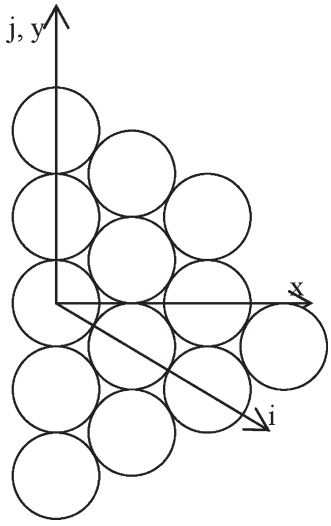

Figure 1. Arrangement of the PS spheres on the substrate.

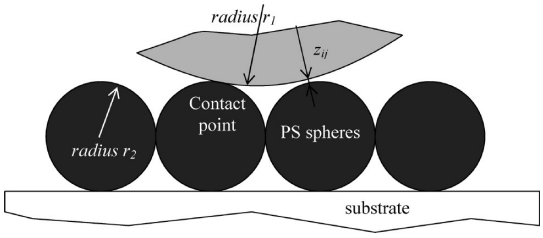

Figure 2. Description of the contact between the probe and the PS spheres on the substrate.

microsphere. An originality of our approach is that the scale where the measurements are done is linked with the microhandling application. The radius of the sphere r_1 is only 10 μm, and the radii of the spheres r_2 are in the nanoscale. Consequently the equivalent radius eq 4 of the contact is usually below several micrometers.

In the microscale and in the nanoscale, it has been shown that mechanical deformation becomes negligible and that adhesion is reduced to the value of interaction forces established in a nondeformable shape as explained by Alvo *et al.*[21] Consequently in nanoscale, adhesion is usually computed using van der Waals equations despite the approaches of the mechanical models DMT or JKR, which are relevant for larger equivalent radius.

The modeling force must be done in the case of one or three contact points. On the basis of a geometrical analysis (Figure 1 and Figure 2), the distance z_{ij} between the probe (r_1) and a sphere (i,j) is, respectively, eq 1 or 2 for one or three contact points:

$$z_{ij_{\min}} = \sqrt{(r_2+z_0+r_1)^2 + 4r_2^2(j^2 - ij + i^2)} - r_1 - r_2 \quad (1)$$

$$z_{ij_{\max}} = \sqrt{(r_2+z_0+r_1)^2 + 4r_2^2(j^2 - ij - i - j + i^2)} - r_1 - r_2 \quad (2)$$

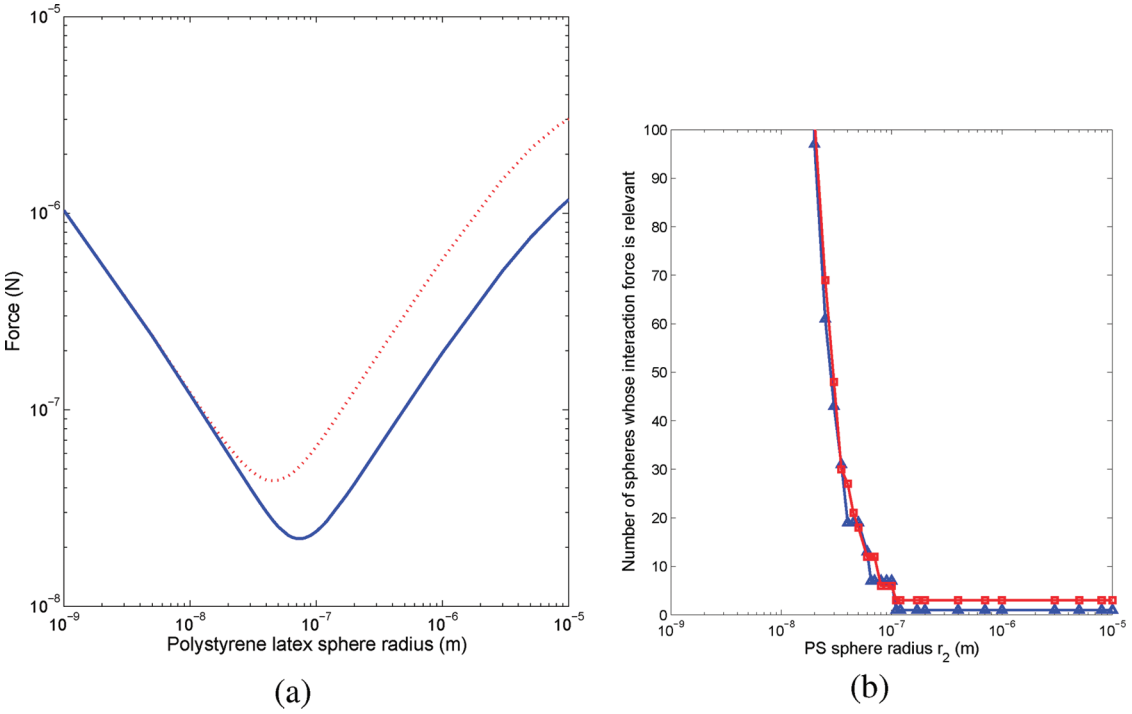

Figure 3. (a) Adhesion force modeling (one contact point, blue solid line; three contact points, red dash line) on the structuring PS surface for 12.5 μm PS sphere radius, r_1, glued on the tipless (z_0 = 0.25 nm); (b) the PS spheres number influencing the adhesion force modeling (threshold 5%) *versus* the PS sphere radius on the structuring surface for one (Δ) and (□) three contact points.

On the basis of Alvo *et al.*,[21] the impact of local deformation on the calculation of the van der Waals force can be neglected in the nanoscale, thus we are considering the force between two rigid spheres. The van der Waals force z_{ij} between the probe and the sphere (i,j) verifies

$$||\vec{F}_{ij}|| = \frac{A_{12}r_{12}}{6z_{ij}^2} \quad (3)$$

where r_{12} is the equivalent radius and A_{12} is the Hamaker constant which can be calculated using the approximative combination law:

$$\frac{1}{r_{12}} = \frac{1}{r_1} + \frac{1}{r_2} \quad (4)$$

$$A_{12} = \sqrt{A_1 A_2} \quad (5)$$

where A_i is the Hamaker constant of the material i.

The total force F_{Tvdw} between an infinite plan structured with PS spheres and the probe is thus

$$F_{\mathrm{Tvdw}} = \sum_{i,j}^{\mathbb{Z}^2} \vec{F}_{ij} \cdot \vec{z} \quad (6)$$

The modeling force for one and three contacts zone can be obtained respectively by

$$F_{\mathrm{Tvdw}_{\min}} = A_{12} \sum_{i,j}^{\mathbb{Z}^2} \frac{r_{12}}{6z_{ij_{\min}}^2} \frac{r_2 + z_0 + r_1}{r_2 + z_{ij_{\min}} + r_1} \quad (7)$$

$$F_{\mathrm{Tvdw}_{\max}} = A_{12} \sum_{i,j}^{\mathbb{Z}^2} \frac{r_{12}}{6z_{ij_{\max}}^2} \frac{\sqrt{(r_2+z_0+r_1)^2 - \left(\frac{4}{3}r_2^2\right)}}{r_2 + z_{ij_{\max}} + r_1} \quad (8)$$

The equation of the pull-off force is function of materials used, through the approximative combination law on Hamaker constant A_{12}, and on the spheres size through the expression on the right side of eq 8. This model of the interaction between a spherical probe and a structured surface has been simulated using the Matlab Simulink software and is presented in Figure 3a for 12.5 μm PS spheres radius on the tipless cantilever *versus* the PS spheres radius on the substrate.

Figure 3a shows the presence of a minimum interaction force which represents an optimum of adhesion reduction in the applicative field of micromanipulation. This minimum is weakly dependent on the contact number. There is 30 nm and 20 nN between the two optima. The second observation is the influence of the initial contact number on the pull-off force and the third is the force increasing after the optimal radius. Indeed, to explain that, it is necessary to determine the number of PS spheres whose interaction force is relevant (Figure 3b). In this case, we consider that the spheres, around the contact point, are a relevant rule on the interactions when they increase the adhesion force of 5%. At the beginning, for PS radius inferior to 10^{-7} m, the neighboring spheres of the contact point do not influence the adhesion force and this last are three times more important for the three contact points. At a radius larger than 10^{-7} m, the spheres close to the contact point modify the pull-off force but with a weaker influence than the sphere at the initial contact point. As seen in Figure 3a, the adhesion forces are the same whatever the number of initial contacts

for a PS sphere radius near 10 nm. With Figure 3b, we can deduce that 100 spheres around the contact point are necessary to obtain the same pull-off force.

RESULTS

The model exposed previously must be validated by the experimental measurements. For that, structuring surfaces with different PS sphere radii was performed and presented as follows. Then, the adhesion force was measured with an AFM, in which a sphere is glued on the tipless cantilever extremity, *versus* the sphere properties: radius (between 35 nm and 2 μm) and nature (borosilicate or carbon). The experimental adhesion forces measured were compared with the previous model. This model cannot be correlated with the sphere mechanical deformation at the moment of the contact between the structuring surface and the cantilever. Indeed, this deformation cannot be evaluated and observed because of the sphere size deposited on the surface.

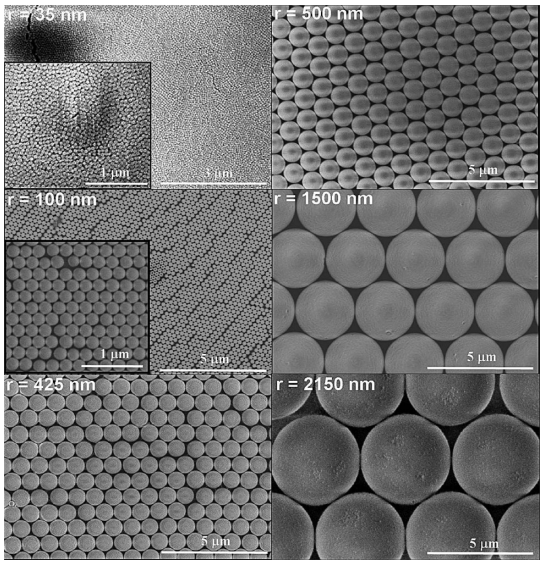

Figure 4. SEM images of a self-assembled monolayer of PS spheres with a radius of (a) 35, (b) 100, (c) 425, (d) 500, (e) 1500, and (f) 2150 nm.

Surface Structuring. Layers of polystyrene PS spheres were created by spin coating PS spheres, radii from 35 nm to 2150 nm (Figure 4), onto Si/SiO_2 substrates. The heating of the structured surface was necessary in order to adhere the particles to the substrate. Indeed, without this step, it is impossible to scan the sample with particles because they moved along the surface.

The layer created is a monolayer. The specimens were successfully coated with large domains of defect-free packing over the entire substrate surface. In Figure 4, the spheres arranged themselves into a close-packed structure of two-dimensional ordered lattices due to attractive capillary forces.

Force Measurement. Six different radii r_2 of PS sphere structuring on silicon wafer have been tested with different borosilicate and carbon spheres r_1, glued on S_a tipless cantilever and measured by SEM. There were 15 measurements performed in different locations on the sample.

Influence of the PS Sphere Size. The force distance measurements obtained, with a borosilicate sphere diameter of 20 μm, for different structured surfaces are presented in Figure 5 and are discussed below.

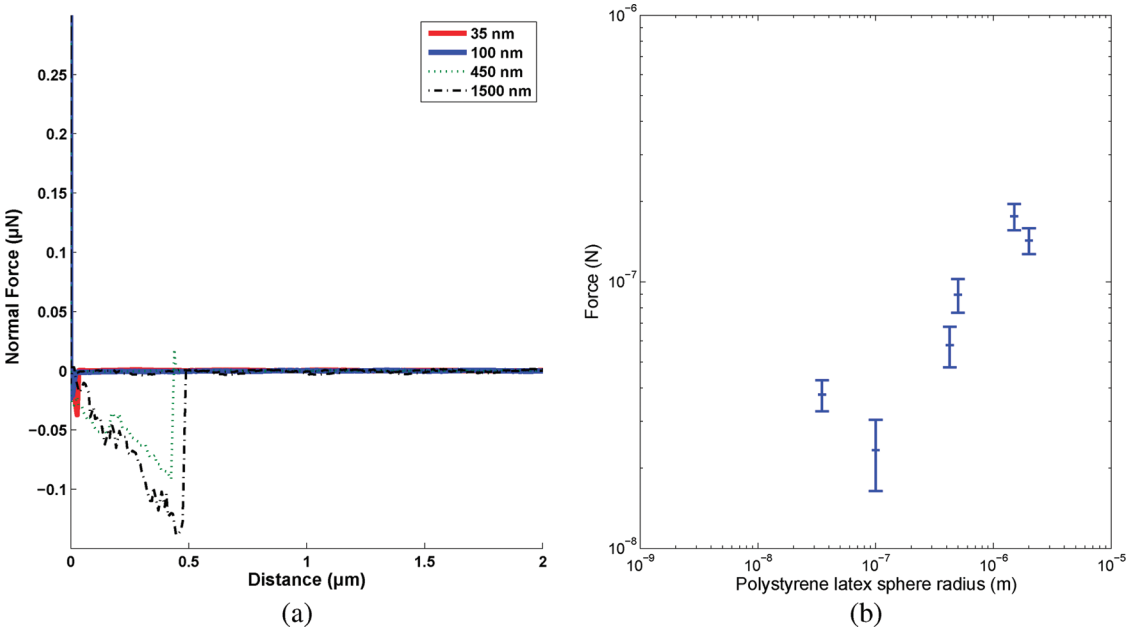

Figure 5. (a) Force−distance curves, for a structuring surface by different PS latex particles sizes with a radius of 35 nm (red line), 100 nm (blue line), 450 nm (green dotted line), and 1.5 μm (black dashed-dotted line); (b) the summary of the measurements. Stiffness = 0.3 N/m and borosilicate radius = 20 μm.

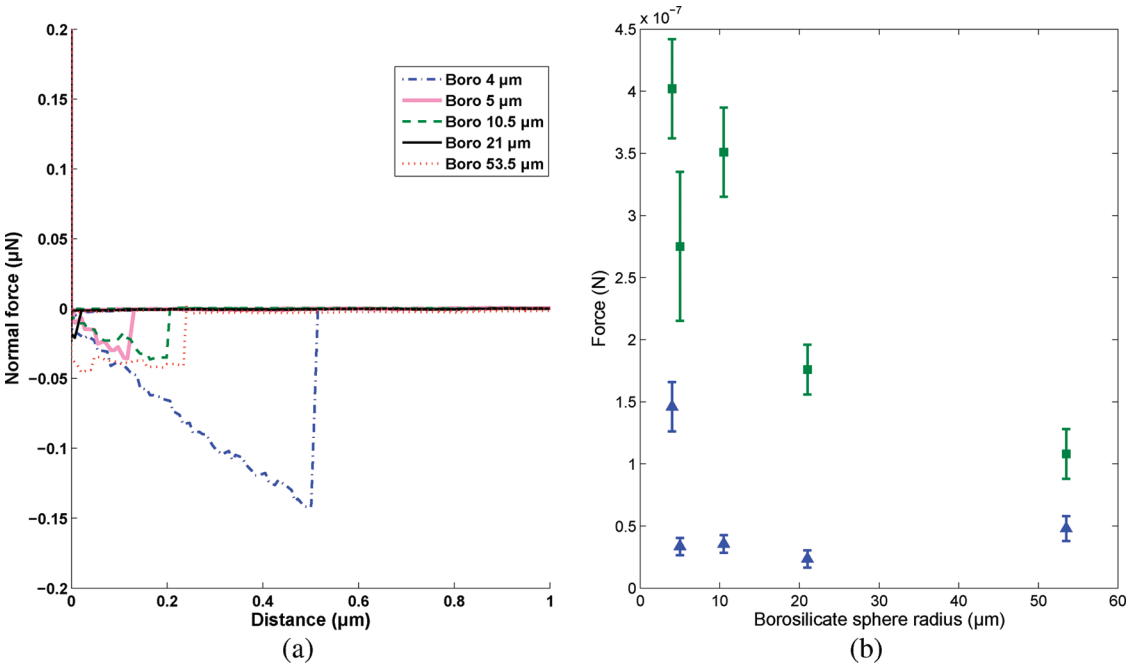

Figure 6. (a) Force–distance curves for a structuring surface with 100 nm PS latex spheres and different borosilicate sphere sizes glued on the tipless: 4 μm (blue dashed-dotted line), 5 μm (pink line), 10.5 μm (green dotted line), 21 μm (black line), 53.5 μm (brown dotted line); (b) the summary of the measurements with all the borosilicate spheres and PS radius 100 nm (▲) and 1500 nm (■). Stiffness = 0.3 N/m.

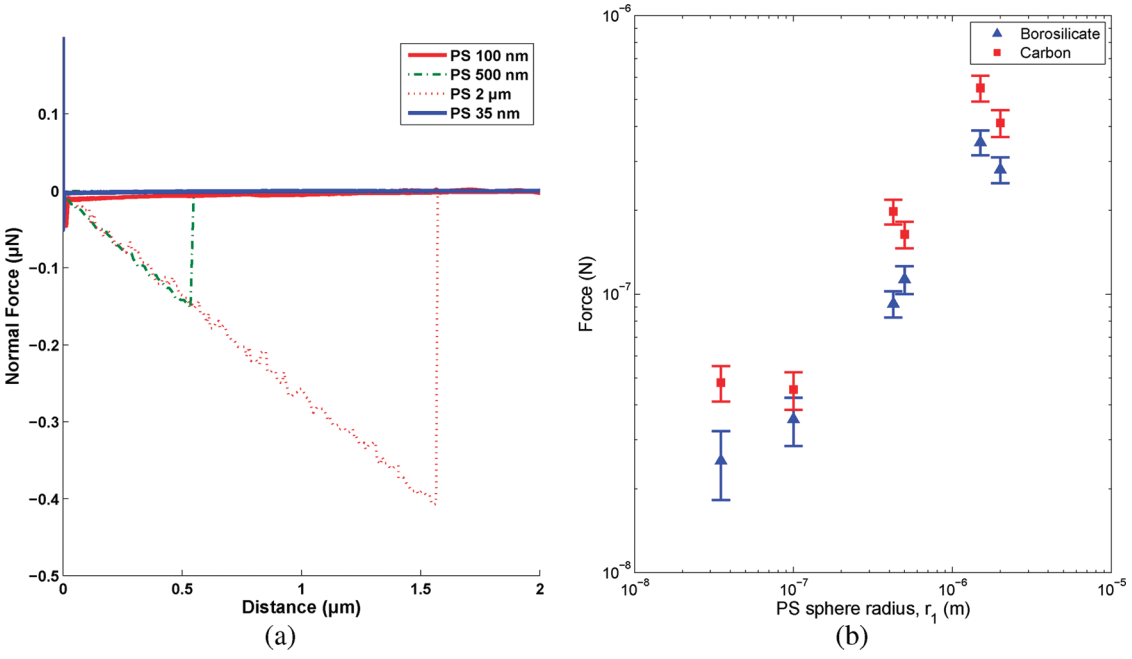

Figure 7. (a) Force–distance curves, for a structured surface by different PS latex particles sizes with a radius of 35 nm (blue line), 100 nm (red line), 500 nm (green dashed-dotted line) and 2 μm (red dotted line); (b) Comparison of the measurements between borosilicate and carbon sphere. Stiffness = 0.3 N/m; borosilicate (▲) and carbon (■) radius = 10.5 and 9 μm, respectively.

In Figure 5, the size of the PS latex particles has an important influence on the adhesion. Indeed, decreasing the size from 2000 nm to a value spread from 35 to 100 nm reduces the adhesion force nearly 10 times. After this value, the adhesion force increases. This shows the existence of an optimal value of the nanostructure radius r_2, which will be explained using the model.

Influence of the Borosilicate Sphere Size. Figure 6 presents the pull-off force measured between a structured surface with the PS radius r_2 100 nm and different borosilicate spheres whose radius r_1 is from 4 to 50 μm.

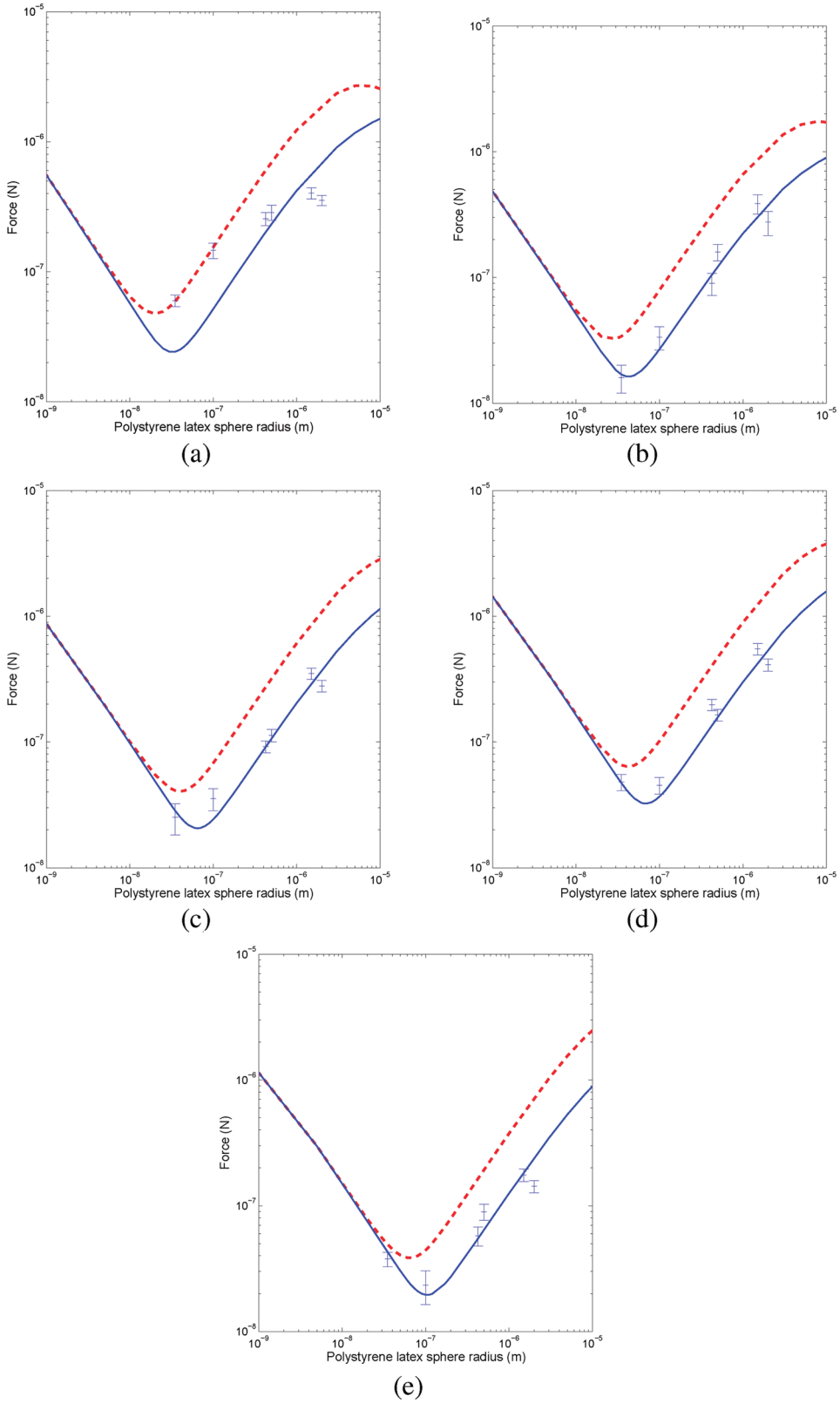

Figure 8. Comparison between the model (one contact point, blue solid line, and three contact points, red dash line) and experimental measurements (error bar) on the structuring surface for different sphere *radii*, r_1, glued on the tipless: (a) borosilicate, 4 μm (z_0 = 0.15 nm); (b) borosilicate, 5 μm (z_0 = 0.21 nm); (c) borosilicate, 10 μm (z_0 = 0.23 nm); (d) carbon, 9 μm (z_0 = 0.30 nm); and (e) borosilicate, 20 μm (z_0 = 0.30 nm).

In Figure 6a,b, the size of the borosilicate sphere S_a influences the pull-off measurements.

Influence of the Material Nature. To validate the model with different material natures, the pull-off force

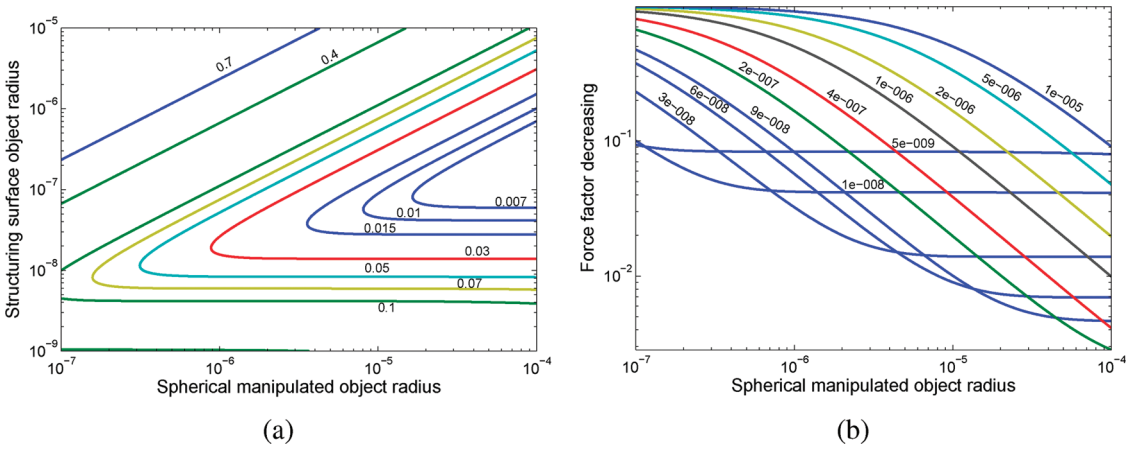

Figure 9. Abacus force for borosilicate probe sphere to (a) determine the decreasing pull-off force or (b) optimize the structured surface. The structure is PS spheres in our case.

measurements were performed on a carbon sphere. Figure 7a presents the results of the measurement with a carbon sphere (radius 10 μm) on the structured surface and Figure 7b compares the results between the borosilicate and the carbon sphere.

In Figure 7b, the sphere composition S_a influences the value of the pull-off force. The adhesion is greater for carbon sphere than borosilicate sphere. This phenomenon is correlated with the Hamaker constant. Indeed, it is A_2 = 500 zJ[52] and A_2 = 65 zJ[21] for, respectively, the carbon and the borosilicate sphere. The van der Waals force, eq 3, based on the combination law, eq 5, increases with the Hamaker constant.

Model and Experimental Measurements Comparison. The model exposed previously is compared with the experimental points of Figure 8. The Hamaker constants are, respectively, A_{12} = 80 zJ and A_{12} = 180 zJ for PS-borosilicate and PS-carbon and are imposed constants for all measurements on the same system. Only the parameter z_0, contact distance, is modified with the diameter of the sphere glued on the tipless extremity. The value range is between 0.15 nm and 0.4 nm. The model of the interaction between a spherical probe and a structured surface has been simulated using the *Matlab Simulink software*.

The experimental point with the borosilicate sphere S_a radius of 50 μm is not shown. Indeed the borosilicate sphere diameter is widely bigger than the cantilever breadth (respectively 100 and 45 μm). So the results obtained with this cantilever cannot be assured and are not presented here. The comparison between value predicted by the model and the measurement, plotted in Figure 8, shows a good concordance. So 90% of the experimental points validate the model. The other 10% of the experimental points are very near to the predicted value, just few nN below the model. The majority of experimental points are on the force modeling with one contact point. The assumption of not taking into account the deformation can only underpredict the force in the model. As the measurements lie on the low end of the predicted adhesion, it seems to validate our assumptions and to show that deformation is negligible at this scale as predicted by Alvo *et al.*[21]

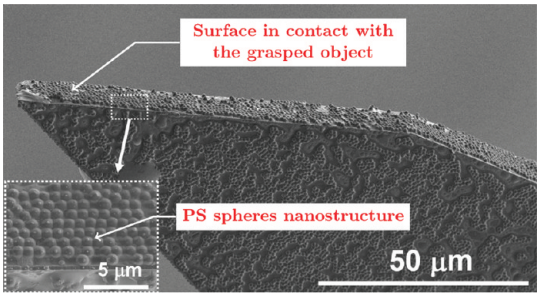

Figure 10. Structuring gripper by PS particles of 1 μm.

TABLE 1. Spin Coating Parameters *versus* the PS Particles Radius

r_2 (nm)	step 1	step 2
35	300 rpm/10 s	2000 rpm/30 s
100	300 rpm/10 s	1000 rpm/30 s
425	300 rpm/10 s	1000 rpm/30 s
500	300 rpm/10 s	500 rpm/30 s
1500	300 rpm/10 s	400 rpm/30 s
2150	200 rpm/10 s	300 rpm/30 s

It is impossible to predict in advance the number of contacts between the probe and the structuring surface because it is impossible to image these contacts. Indeed, the small size of the PS spheres requires SEM observations, the contact must be observed with a lateral view, and there is no SEM with lateral view. Furthermore, the PS deposited planarity is not perfect, and the sphere probe, being bigger than the PS deposit, creates a shadowing area that obstructs the contact imaging. Moreover SEM observations are performed under vacuum. These conditions are not adapted to our controlled environment (humidity 30%).

The adhesion force obtained with the structuring surface is below that of a silicon substrate plane, where the adhesion is near 1 μN. Indeed, with the structured

surface, the minimal force is near 10 μN and is decreased 100 times. In our experimental case, the optimum radius r_2 to minimize the adhesion is between 35 and 70 nm. This value depends of the diameter of the borosilicate sphere glued to the cantilever. For object manipulation where the size is known, a small variation of the PS sphere radius, deposited on the gripper and near the minimal pull-off force, does not drastically modify the adhesion force.

DISCUSSION

The proposed model can be used to determine the diameter of the optimal particles spheres to be placed on a gripper to minimize adhesion force with a grasped sphere S_a. The model is useful whatever the manipulated objects and deposited spheres material nature are.

The decreasing pull-off force ($f(r_1, r_2, z_0)$, equation12), obtained after surface structuring against the surface plane ($F_{vdw_{plane}}$, eq 11), can be evaluated from eq 7 or 8. In the following, and with the observations of Figure 8, eq 7 is modified:

$$F_{Tvdw_{min}} = \frac{A_{12}r_1}{6z_0^2}\frac{r_{12}}{r_1}\sum_{i,j}^{\mathbb{Z}^2}\frac{z_0^2}{z_{ij_{min}}^2}\frac{r_2+z_0+r_1}{r_2+z_{ij_{min}}+r_1} \quad (9)$$

$$F_{Tvdw_{min}} = F_{vdw_{plane}} f(r_1, r_2, z_0) \quad (10)$$

where:

$$F_{vdw_{plane}} = \frac{A_{12}r_1}{6z_0^2} \quad (11)$$

$$f(r_1, r_2, z_0) = \frac{r_{12}}{r_1}\sum_{i,j}^{\mathbb{Z}^2}\frac{z_0^2}{z_{ij_{min}}^2}\frac{r_2+z_0+r_1}{r_2+z_{ij_{min}}+r_1} \quad (12)$$

If the manipulated object size is known, the decreasing pull-off force can be determined if the radius of the spheres on the structured surface is imposed (Figure 9a) or the structured surface is adapted to optimize the decreasing pull-off force (Figure 9b) with the abacus curve.

With Figure 9 and the eq 9, the researchers can control the pull-off force *via* changes in the nature and the size of the material in a predictable manner.

Experimentally, some PS spheres have been deposed on silicon grippers[53] (Figure 10). SEM images shows that PS spheres self-assembled into colloidal crystals which were close-packed structures with three-dimensional ordered lattices *via* attractive capillary forces on Si grippers. These preliminary experiments show the feasibility of using natural lithography for patterning nonplanar complex Si grippers' tools with an extremely straightforward and simple method. More experiments are in progress in order to use these structured grippers for micro- and nanomanipulation.

CONCLUSION

In this paper, we have studied the interaction behavior, and most precisely the adhesion force, between a structured surface and carbon or borosilicate spheres. The experiments were performed as a function of the polystyrene latex particle radii from 35 to 2000 nm deposited on the silica substrate, and of radii and nature of the spheres glued on the tipless extremity. The experimental measurements were compared to a multisphere van der Waals model and show a good agreement. For a fixed sphere, the pull-off force decreases with the PS radius until a fixed value before it begins to increase. The PS radius values for the minimal pull-off force are a function of the sphere radius glued on the tipless cantilever, varied from 40 nm to 100 nm in our conditions.

Because adhesion is the current highest disturbance in micromanipulation (positioning and releasing), a structured surface is a promising way to improve micro-object manipulation in the future. With the model presented, the size of the polystyrene spheres deposited can be optimized as a function of the manipulated object material size and nature. This paper provides design rules to structure a gripper surface in order to minimize adhesion. A wide range of applications, in the field of telecommunications, bioengineering, and more generally speaking MEMS can be also envisaged for these structured microgrippers.

MATERIALS AND METHODS

Surface Structuring. Different sizes (radius, r_2, between 35 nm and 2 μm) of commercially available PS microsphere (noted S_b) suspension were used (Polysciences, Inc., Eppelheim, Germany) as received. Acetone, H_2SO_4(25%), and H_2O_2 (30%) were purchased from Aldrich, and p-type Si wafers (5−10 Ω·cm, (111) crystal orientation) of dimensions 1.5 cm^2 from Silicon Materials were used as substrates. The deposit method was presented in a previous paper.[26] The different parameters of the spin coating were detailed in Table 1. After spin coating, the PS spheres organized on the *Si* substrate were characterized by Scanning Electron Microscopy (*SEM*, Hitachi, S-4800).

Grippers Structuring. Si microgrippers[53] were precleaned in acetone for 5 min and 1 wt % hydrofluoric acid (HF) for 5 min to remove organic contamination and native oxide on their surface. Then, precleaned Si grippers were immersed in H_2SO_4/H_2O_2 (1/1) solution overnight to achieve hydrophilic surface. The gripper was dropped in a monodisperse suspension of polystyrene (PS) microspheres (1 μm in diameter) and dried in air overnight. The grippers were characterized by scanning electron microscopy (SEM, Hitachi, S-4800).

Force Distance Measurement by Atomic Force Microscopy. Characterization of the pull-off force was performed with a commercial atomic force microscope (stand-alone SMENA scanning probe microscope NT-MDT). The experiments were done under a

controlled environment with a laminar flow (humidity 30% and 25 °C) on the Nanorol platform station. The "Nanorol platform" can be used by external person (http://nanorol.cnrs.fr/events.php). The rectangular silicon AFM cantilever, whose stiffness is 0.3 N/m, was fixed, and the substrate moved vertically. The same kind of cantilever was used for all experiments. As the objective of this work is to improve the reliability of micro-object manipulation, interactions have been studied between a micrometric sphere and a structuring surface. Measurements were in fact performed with a cantilever where a sphere (r_1) was glued in place of the standard AFM tip, noted S_a. The size and the nature of the sphere were determined by the experimenter. The force calibration was performed for each cantilever with this resonance frequency, and 10 measurements were done at different locations on the same sample with a driving speed of 200 nm/s.

Spheres Glued on the Cantilever. All borosilicate spheres are provided by SPI Supplies and commercialized by Neyco (Paris, France). Diameters are certified using certified standards from the National Institute of Standards and Technology (NIST). The glassy carbon sphere, Sigradur K, is supplied by HTW (Germany). The power is spherical and the diameter is between 10 and 20 μm. Before experiment the carbon sphere gluing on the cantilever is measured in SEM. The glass spheres gluing has been performed in the laboratory with the Dymax 628-VLV glue and the Blue Wave 50 apparatus (Dymax, Garches, France). The glue was reticulated by UV light (365 nm).

Acknowledgment. This work was partially supported by the EU under HYDROMEL, Contract NMP2-CT-2006-026622 (Hybrid ultraprecision manufacturing process based on positional- and self-assembly for complex microproducts); FAB2ASM, Contract FoF-NMP-2010-260079 (Efficient and precise 3D integration of heterogeneous microsystems from fabrication to assembly); and by the French National Agency (ANR) under NANOROL, Contract ANR-07-ROBO-0003, (Nanoanalyse for micromanipulation). We would also like to acknowledge the support of D. Rostoucher, FEMTO-ST, for sphere joining on the tipless cantilever extremity.

REFERENCES AND NOTES

1. Tamadazte, B.; Dembélé, S.; Le Fort-Piat, N. A Multiscale Calibration of a Photon Videomicroscope for Visual Servo Control: Application to MEMS Micromanipulation and Microassembly. *Sens. Transducers J.* **2009**, *5*, 37–52.
2. Lambert, P. *Capillary Forces in Micro-assembly*; Springer: Amsterdam, The Netherlands, 2008.
3. Gauthier, M.; Régnier, S.; Rougeot, P.; Chaillet, N. Forces Analysis for Micromanipulations in Dry and Liquid Media. *J. Micromechatronics* **2006**, *3*, 389–413.
4. Zhou, Q.; Chang, B.; Koivo, H. N. Ambient Environment Effects in Micro/Nano Handling. Proceedings of the International Workshop on Microfactories, Shangai, China, Oct. 15−17, 2004; IOP Publishing Ltd.: Bristol, U.K., 2004; pp 146−151.
5. Hériban, D.; Gauthier, M. Robotic Micro-Assembly of Microparts Using a Piezogripper. Proceedings of the 2008 IEEE/RSJ International Conference on Intelligent Robots and Systems, Nice, France, Sept 22−26, 2008; IEEE: Piscataway, NJ, 2008; pp 4042−4047.
6. Dafflon, M.; Lorent, B.; Clavel, R. A Micromanipulation Setup for Comparative Tests of Microgrippers. *International Symposium on Robotics (ISR)*, Münich, Germany, May 15-17, 2006.
7. Blomberg, E.; Poptoshev, E.; Claesson, P. M.; Caruso, F. Surface Interactions during Polyelectrolyte Multilayer Buildup. 1. Interactions and Layer Structure in Dilute Electrolyte Solutions. *Langmuir* **2004**, *20*, 5432–5438.
8. Charrault, E.; Gauthier, C.; Marie, P.; Schirrer, R. Experimental and Theoretical Analysis of a Dynamic JKR Contact. *Langmuir* **2009**, *25*, 5847–5854.
9. Dejeu, J.; Rougeot, P.; Gauthier, M.; Boireau, W. Reduction of Micro-object's Using Chemical Functionalisation. *Micro Nano Lett.* **2009**, *4*, 74–79.
10. Wang, T.; Canetta, E.; Weerakkody, T. G.; Keddie, J. L. Nanomaterials: Sticky but Not Messy. *ACS Appl. Mater. Interfaces* **2009**, *1*, 631–639.
11. Gong, H.; Garcia-Turiel, J.; Vasilev, K.; Vinogradova, O. I. Interaction and Adhesion Properties of Polyelectrolyte Multilayers. *Langmuir* **2005**, *21*, 7545–7550.
12. Rabenorosoa, K.; Clevy, C.; Lutz, P.; Gauthier, M.; Rougeot, P. Evaluation of Pull-off Forces for Planar Contact in Micro-assembly. *Micro Nano Lett.* **2009**, *4*, 148–154.
13. Vajpayee, S.; Hui, C.-Y.; Jagota, A. Model-Independent Extraction of Adhesion Energy from Indentation Experiments. *Langmuir* **2008**, *24*, 9401–9409.
14. Murphy, M. P.; Kim, S.; Sitti, M. Enhanced Adhesion by Gecko-Inspired Hierarchical Fibrillar Adhesives. *ACS Appl. Mater. Interfaces* **2009**, *1*, 849–855.
15. Johnson, K. L.; Kendall, K.; Roberts, A. D. Surface Energy and the Contact of Elastic Solids. *Proc. R. Soc. London, Ser. A* **1971**, *324*, 301–313.
16. Derjaguin, B. V.; Muller, V.; Toporov., Y. P. Effect of Contact Deformations on the Adhesion of Particles. *J. Colloid Interface Sci.* **1975**, *53*, 314–326.
17. Maugis, D. Adhesion of Spheres: The JKR-Transition Using a Dugdale Model. *J. Colloid Interface Sci.* **1992**, *150*, 243–269.
18. Jones, R.; Pollock, H. M.; Cleaver, J. A. S.; Hodges, C. S. Adhesion Forces between Glass and Silicon Surfaces in Air Studied by AFM: Effects of Relative Humidity, Particle Size, Roughness, and Surface Treatment. *Langmuir* **2002**, *18*, 8045–8055.
19. Hamaker, H. C. The London−van der Waals Attraction between Spherical Particules. *Physica* **1937**, *4*, 1058–1072.
20. Delrio, F. W.; de Boer, M.; Knapp, J.; Davidreedy, E.; Clews, P.; Dunn, M. The Role of van der Waals Forces in Adhesion of Micromachined Surfaces. *Nat. Mater.* **2005**, *4*, 629–634.
21. Alvo, S.; Lambert, P.; Gauthier, M.; Régnier, S. Adhesion Model for Micromanipulation Based on van der Waals Forces. *J. Adhes. Sci. Technol.* **2010**, *24*, 2415–2428.
22. Jaiswal, R. P.; Kumar, G.; Kilroy, C. M.; Beaudoin, S. P. Modeling and Validation of the van der Waals Force During the Adhesion of Nanoscale Objects to Rough Surfaces: a Detailed Description. *Langmuir* **2009**, *25*, 10612–10623.
23. Thoreson, E.; Martin, J.; Burnham, N. The Role of Few-Asperity Contacts in Adhesion. *J. Colloid Interface Sci.* **2006**, *298*, 94–101.
24. Li, Q.; Rudolph, V.; Peukert, W. London−van der Waals Adhesiveness of Rough Particles. *Powder Technol.* **2006**, *161*, 248–255.
25. Hodges, C. S.; Cleaver, J. A. S.; Ghadiri, M.; Jones, R.; Pollock, H. M. Forces between Polystyrene Particles in Water Using the AFM: Pull-Off Force *vs* Particle Size. *Langmuir* **2002**, *18*, 5741–5748.
26. Dejeu, J.; Bechelany, M.; Philippe, L.; Rougeot, P.; Michler, J.; Gauthier, M. Reducing the Adhesion between Surfaces Using Surface Structuration with PS Latex Particle. *ACS Appl. Mater. Interfaces* **2010**, *2*, 1630–1636.
27. Dejeu, J.; Rougeot, P.; Gauthier, M.; Boireau, W. Adhesions Forces Controlled by Chemical Self-Assembly and pH, Application to Robotic Microhandling. *ACS Appl. Mater. Interfaces* **2009**, *1*, 1966–1973.
28. Lupu, S.; Lakard, B.; Hihn, J.; Dejeu, J.; Rougeot, P.; Lallemand, S. Morphological Characterization and Analytical Application of Poly(3,4-ethylenedioxythiophene)-Prussion Blue Composite Films Electrodeposited *in Situ* on Platinum Electrode Chips. *Thin Solid Films* **2011**in press.
29. Dejeu, J.; Taouil, A. E.; Rougeot, P.; Lakard, S.; Lallemand, F.; Lakard, B. Morphological and Adhesive Properties of Polypyrrole Films Synthesized by (Sono)electrochemistry. *Synth. Met.* **2010**, *160*, 2540–2545.
30. Dejeu, J.; Rougeot, P.; Gauthier, M.; Boireau, W. Robotic Submerged Microhandling Controlled by pH Switching. Proceedings of the IEEE IEEE/RSJ 2009 International Conference on Intelligent Robots and Systems, St Louis, October 11−15, 2009.
31. Dejeu, J.; Rougeot, P.; Gauthier, M.; Boireau, W. Improvement of Robotic Micromanipulations Using Chemical

Functionalisations. *IPAS 2010 (International Precision Assembly Seminar), IFIP AICT 315* **2010**, 215–221.
32. Sausse Lhernould, M. S.; Delchambre, A.; Régnier, S.; Lambert, P. Electrostatic Forces in Micromanipulations: Review of Analytical Models and Simulations Including Roughness. *Appl. Surf. Sci.* **2007**, *253*, 6203–6210.
33. Persson, B. N. J. Adhesion between an Elastic Body and a Randomly Rough Hard Surface. *Eur. Phys. J. E: Soft Matter Biol. Phys.* **2002**, *8*, 385–401.
34. Sahoo, P.; Chowdhury, S. K. R. A Fractal Analysis of Adhesive Wear at the Contact between Rough Solids. *Wear* **2002**, *253*, 924–934.
35. Li, J.; Fu, J.; Cong, Y.; Wu, Y.; Xue, L. J.; Han, Y. C. Macroporous Fluoropolymeric Films Templated by Silica Colloidal Assembly: A Possible Route to Superhydrophobic Surfaces. *Appl. Surf. Sci.* **2006**, *252*, 2229–2234.
36. Kim, S. H.; Kim, J. H.; Kang, B. K.; Uhm, H. S. Superhydrophobic CFx Coating via In-Line Atmospheric RF Plasma of He-CF_4-H_2. *Langmuir* **2005**, *21*, 12213–12217.
37. Han, J. T.; Zheng, Y.; Cho, J. H.; Xu, X.; Cho, K. Stable Superhydrophobic Organic−Inorganic Hybrid Films by Electrostatic Self-Assembly. *J. Phys. Chem. B* **2005**, *109*, 20773–20778.
38. Zhao, N.; Shi, F.; Wang, Z. Q.; Zhang, X. Combining Layer-by-Layer Assembly with Electrodeposition of Silver Aggregates for Fabricating Superhydrophobic Surfaces. *Langmuir* **2005**, *21*, 4713–4716.
39. Shi, F.; Wang, Z. Q.; Zhang, X. Combining a Layer-by-Layer Assembling Technique with Electrochemical Deposition of Gold Aggregates to Mimic the Legs of Water Striders. *Adv. Mater.* **2005**, *17*, 1005–1009.
40. Hikita, M.; Tanaka, K.; Nakamura, T.; Kajiyama, T.; Takahara, A. Super-Liquid-Repellent Surfaces Prepared by Colloidal Silica Nanoparticles Covered with Fluoroalkyl Groups. *Langmuir* **2005**, *21*, 7299–7302.
41. Jiang, L.; Zhao, Y.; Zhai, J. A Lotus-Leaf-like Superhydrophobic Surface: A Porous Microsphere/Nanofiber Composite Film Prepared by Electrohydrodynamics. *Angew. Chem., Int. Ed.* **2004**, *43*, 4338–4341.
42. Gu, Z. Z.; Wei, H. M.; Zhang, R. Q.; Han, G. Z.; Pan, C.; Zhang, H.; Tian, X. J.; Chen, Z. M. Artificial Silver Ragwort Surface. *Appl. Phys. Lett.* **2005**, *86*, 201915–201915−3.
43. Deckman, H.; Dunsmuir, J. Natural Lithography. *Appl. Phys. Lett.* **1982**, *41*, 377–379.
44. Sakamoto, S.; Philippe, L.; Bechelany, M.; Michler, J.; Asoh, H.; Ono, S. Ordered Hexagonal Array of Au Nanodots on Si Substrate Based on Colloidal Crystal Templating. *Nanotechnology* **2008**, *19*, 405304–405309.
45. Bechelany, M.; Brodard, P.; Philippe, L.; Michler, J. Extended Domains of Organized Nanorings of Silver Grains as Surface-Enhanced Raman Scattering Sensors for Molecular Detection. *Nanotechnology* **2009**, *20*, 455302–455309.
46. Bechelany, M.; Maeder, X.; Riesterer, J.; Hankache, J.; Lerose, D.; Christiansen, S.; Michler, J.; Philippe, L. Synthesis Mechanisms of Organized Gold Nanoparticles: Influence of Annealing Temperature and Atmosphere. *Cryst. Growth Des.* **2010**, 587–596.
47. Mook, W.; Niederberger, C.; Bechelany, M.; Philippe, L.; Michler, J. Compression of Freestanding Gold Nanostructures: From Stochastic Yield to Predictable Flow. *Nanotechnology* **2010**, *21*, 55701.
48. Bechelany, M.; Brodard, P.; Elias, J.; Philippe, L.; Michler, J. Simple Synthetic Route for SERS Active Gold Nanoparticles Substrate with Controlled Shape and Organization. *Langmuir* **2010**, *26*, 14364–14371.
49. Elias, J.; Lévy-Clément, C.; Bechelany, M.; Michler, J.; Wang, G.-Y.; Wang, Z.; Philippe, L. Hollow Urchin-like ZnO Thin Films by Electrochemical Deposition. *Adv. Mater.* **2010**, *22*, 1607–1612.
50. Lerose, D.; Bechelany, M.; Philippe, L.; Michler, J.; Christiansen, S. Ordered Arrays of Epitaxial Silicon Nanowires Produced by Nanosphere Lithography and Chemical Vapor Deposition. *J. Cryst. Growth* **2010**, *312*, 2887–2891.
51. Yoon, T.; Lee, H.; Yan, J.; Kim, D. Fabrication of SiC-Based Ceramic Microstructures from Preceramic Polymers with Sacrificial Templates and Lithographic Techniques—A Review. *J. Ceram. Soc. Jpn. Int. Ed.* **2006**, *114*, 473–479.
52. Parfitt, G.; Picton, N. Stability of Dispersions of Graphitized Carbon Blacks in Aqueous Solutions of Sodium Dodecyl Dulphate. *Trans. Faraday Soc.* **1968**, *64*, 1955–1964.
53. Agnus, J.; Hériban, D.; Gauthier, M.; Pétrini, V. Silicon End-Effectors for Micrograpping Tasks. *Precis. Eng.* **2009**, *33*, 542–548.